PHYSICAL REVIEW B **93**, 245147 (2016)

Pseudogap and superconductivity in two-dimensional doped charge-transfer insulators

L. Fratino,[1] P. Sémon,[2] G. Sordi,[1] and A.-M. S. Tremblay[2,3]
[1]*Department of Physics, Royal Holloway, University of London, Egham, Surrey TW20 0EX, United Kingdom*
[2]*Département de Physique and Regroupement Québéquois sur les Matériaux de Pointe, Université de Sherbrooke, Sherbrooke, Québec, Canada, J1K 2R1*
[3]*Canadian Institute for Advanced Research, Toronto, Ontario, Canada, M5G 1Z8*
(Received 27 February 2016; revised manuscript received 18 April 2016; published 24 June 2016)

High-temperature superconductivity emerges upon doping a state of matter that is insulating because of interactions. A widely studied model considers one orbital per CuO_2 unit cell on a square lattice with a strong intraorbital repulsion that leads to a so-called Mott-Hubbard insulator. Here we solve a model that takes into account, within each unit cell, two oxygen orbitals where there is no electron-electron repulsion and a copper orbital with strong electron-electron repulsion. The insulating phase is a so-called charge-transfer insulator, not a Mott-Hubbard insulator. Using cluster dynamical mean-field theory with continuous-time quantum Monte Carlo as an impurity solver and 12 atoms per cluster, we report the normal and superconducting phase diagram of this model as a function of doping, interaction strength, and temperature. As expected, the three-orbital model is consistent with the experimental observation that doped holes are located predominantly on oxygens, a result that goes beyond the one-orbital model. Nevertheless, the phase boundary between pseudogap and correlated metal, the Widom line, and the origin of the pairing energy (kinetic vs potential) are similar to the one-orbital model, demonstrating that these are emergent phenomena characteristic of doped Mott insulators, independently of many microscopic details. Broader implications are discussed.

DOI: 10.1103/PhysRevB.93.245147

The appearance of high-temperature superconductivity upon doping an interaction-driven insulator is one of the most surprising phenomena in nature. A major goal of research in that field is to chart the phase diagram in the hope of providing key insights into an unconventional pairing mechanism and into the nature of the strongly correlated states of matter observed. With experiments driving this quest, and revealing a complex phase diagram [1], theory is challenged to provide a framework to explain such complexity. The challenge comes from the fact that the insulating phase that is doped arises from interactions so strong [2] that tools to describe such a nonperturbative regime are needed. Significant progress has been made in this area by novel theoretical approaches such as cluster extensions [3–5] of dynamical mean-field theory (DMFT) [6].

The physics that must be understood is that of a square lattice made of CuO_2 unit cells where electrons on copper interact strongly. Intense effort devoted to study the case of a single orbital per unit cell with an on-site repulsion, i.e., the two-dimensional Hubbard model, has shown that this simple model captures the basic phenomenology of cuprates [7,8].

A more realistic model for the cuprates includes three orbitals per CuO_2 unit cell [9,10]. The necessity of this model is demonstrated by numerous experiments that show that doped holes are found on oxygen [11]. The ability to delocalize on oxygen allows electrons to feel a much weaker effective interaction, but at one hole per unit cell and strong enough repulsion on copper, one obtains a charge-transfer insulator [12]. It is this kind of interaction-driven insulator of the three-orbital model that becomes a high-temperature superconductor upon doping. Hence this is the model we study.

Previous single-site DMFT calculations [13–21] provided important insights on the phase diagram. However, the inclusion of short-range correlations is still a formidable theoretical problem. Despite pioneering investigations using cluster methods [22–25], the precise form of the temperature-doping T-δ phase diagram is largely unexplored and several of its key aspects are uncertain. Notably, the finite temperature behavior of the metal to charge-transfer insulator transition driven by hole doping is unknown.

Here we chart the cellular DMFT solution of the whole T-δ phase diagram of a doped charge-transfer insulator. We focus on four possible phases of the model, namely, the charge-transfer insulator, the pseudogap, the correlated metal, and a d-wave superconducting state, along with their phase boundaries. Our goal is to establish if the basic phenomenology of cuprates found in the one-orbital model survives in the more realistic three-orbital model and which phenomena are emergent, i.e., independent of such details as number of orbitals per unit cell, shape of the Fermi surface, redistribution of spectral weight, and location of holes within the unit cell.

I. MODEL AND METHOD

We consider the three-band Hamiltonian for copper $3d_{x^2-y^2}$ and oxygen $2p_x$,$2p_y$ orbitals. Ordering the corresponding annihilation operators as $(d_{\mathbf{k}\sigma}, p_{x,\mathbf{k}\sigma}, p_{y,\mathbf{k}\sigma})$, where $\mathbf{k}$ is the wave vector and σ the spin, the noninteracting part of the Hamiltonian for the infinite lattice reads [26]

$$\mathbf{h}_0(\mathbf{k}) = \begin{pmatrix} \epsilon_d & V_{dp_x} & V_{dp_y} \\ V_{dp_x}^\dagger & \epsilon_p + W_{p_xp_x} & W_{p_xp_y} \\ V_{dp_y}^\dagger & W_{p_xp_y}^\dagger & \epsilon_p + W_{p_yp_y} \end{pmatrix}, \quad (1)$$

with $V_{dp_x} = t_{pd}(1 - e^{ik_x})$, $V_{dp_y} = t_{pd}(1 - e^{ik_y})$, $W_{p_xp_x} = 2t_{pp}(\cos k_x - 1)$, $W_{p_yp_y} = 2t_{pp}(\cos k_y - 1)$, and $W_{p_xp_y} = t_{pp}(1 - e^{-ik_x})(1 - e^{ik_y})$. Here t_{pd} (t_{pp}) is the oxygen-copper (oxygen-oxygen) hopping amplitude, and ϵ_d (ϵ_p) is the copper (oxygen) on-site energy. The copper-copper distance and t_{pp} are taken as unity. $\mathbf{h}_0$ leads to the Fermi surface observed

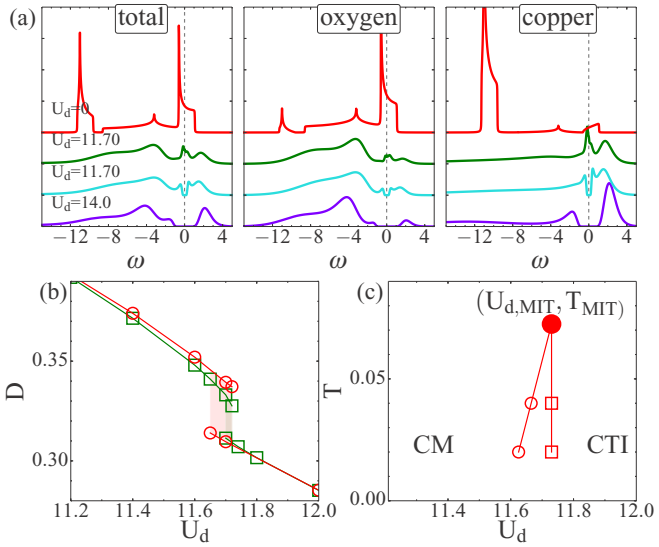

FIG. 1. (a) Local density of states $N(\omega)$ at $n_{\rm tot} = 5$ and $\beta = 50$ for several values of U_d. From left to right: total, projected $N(\omega)$ on the p and d orbitals. Other model parameters are $|\epsilon_p - \epsilon_d| = 9, t_{pp} = 1$, and $t_{pd} = 1.5$. (b) Double occupancy D as a function of U_d at $n_{\rm tot} = 5$ for $\beta = 25$ (squares) and $\beta = 50$ (circles). Hysteresis region is shaded. (c) T versus U_d phase diagram at $n_{\rm tot} = 5$. A first-order transition at finite U_d between a correlated metal (CM) and a charge-transfer insulator (CTI) is bounded by the jumps in the double occupancy and terminates at a critical end point.

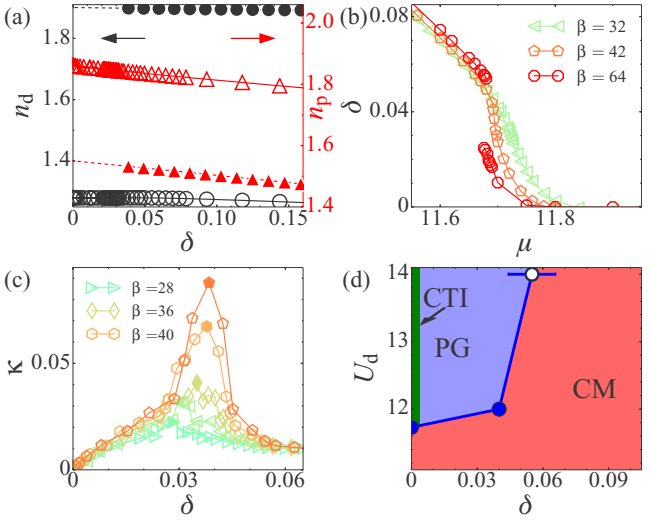

FIG. 2. (a) Partial occupation n_d (circles), n_p (triangles) versus $\delta = 5 - n_{\rm tot}$ at $\beta = 25$ and $U_d = 0, 12$ (full and open symbols, respectively). (b) δ versus μ for $U_d = 12$, for different temperatures. A plateau at $\delta(\mu) = 0$ signals the CTI. Hysteresis appears at finite doping at the lowest T. (c) Charge compressibility κ versus δ for different temperatures at $U_d = 12$. κ diverges at the end point (δ_p, T_p) of the PG-CM first-order transition. (d) U_d versus δ phase diagram. The boundary between CTI and PG is second order. The boundary between CTI and CM at $\delta = 0$ is first order. The green line is drawn at $T = T_{\rm MIT}$. The boundary between PG and CM is first order. The blue line denotes δ_p versus U_d. Since T_p decreases with increasing U_d, we show as blue solid circles the position δ_p of the end points and as blue open circle the position of $\kappa_{\rm max}$ at our lowest T. The full data set for (b) and (c) is in SM Fig. 3 and Fig. 4. respectively [27]. Model parameters are $|\epsilon_p - \epsilon_d| = 9$, $t_{pp} = 1$, and $t_{pd} = 1.5$.

experimentally in the overdoped region of the cuprates (see Supplemental Material (SM) Fig. 2 [27]). For the interacting part, only the on-site repulsion on d orbitals U_d is retained.

We solve this model with cellular dynamical mean-field theory (CDMFT), which isolates a cluster of 12 lattice sites with $(N_d, N_p) = (4,8)$ and replaces the missing lattice environment by a self-consistent noninteracting bath. The cluster plus bath impurity model is solved with continuous-time quantum Monte Carlo for the hybridization expansion [28]. (See SM Sec. I for details [27].)

II. OPENING OF THE CHARGE-TRANSFER GAP

As described by the Zaanen-Sawatzky-Allen scheme [12] (ZSA), this model accounts for different correlated insulating states when the total occupation is $n_{\rm tot} = n_d + 2n_p = 5$ (one hole per CuO_2 unit): the charge-transfer insulator and the Mott-Hubbard one. The former is relevant for the cuprates and is the focus of the present work.

Figure 1(a) shows the local density of states (DOS) $N(\omega) = -1/\pi \,\mathrm{Im}G(\omega)$ at $n_{\rm tot} = 5$ for several values of U_d at the inverse temperature $\beta = 50$ (from left to right: total, projected DOS on the p and d orbitals). The zero of energy is the Fermi level. To set the system in the charge-transfer regime, we take $\epsilon_d = 0$ and $\epsilon_p = 9$ so that the localized d orbital is beneath the oxygen band. The bandwidth originating from t_{pp} alone is 8. By virtue of the hybridization term, here $t_{pd} = 1.5$, the d electrons acquire a finite dispersion, and, for the noninteracting case, form a narrow band centered at $\omega \approx -11$. (See upper red curve and SM Sec. I [27]). As described by the ZSA scheme [12], for $U_d > |\epsilon_p - \epsilon_d|$ and $|\epsilon_p - \epsilon_d| > t_{pd}$ a correlation gap opens up and the system becomes a charge-transfer insulator. The lower violet curve shows this dramatic effect of correlations. At low temperature, the interaction-driven transition between the metal and the charge-transfer insulator is first order. At intermediate values of U_d, there is a coexistence between a metallic and insulating solutions to the CDMFT equations (green and blue curve, respectively).

The first-order nature of the transition is best shown by the double occupancy D of d orbitals as a function of U_d [cf Fig. 1(b)]. D shows hysteresis loops between two solutions, with sudden jumps at $U_{d,c1}(T)$, where the insulating solution ceases to exists, and at $U_{d,c2}(T)$, where the metallic solution disappears. Hysteresis loops become wider with decreasing T. The behavior of D allows us to construct the temperature versus U_d phase diagram in Fig. 1(c). The first-order transition between a correlated metal and a charge-transfer insulator occurs within the coexistence region, bounded by the spinodals $U_{d,c1}$ and $U_{d,c2}$ (open circles and squares, respectively), and terminates in a critical end point, where dD/dU_d diverges. Our results extend to finite temperature the previously obtained $T = 0$ phase diagram [25].

III. HOLE-DOPING-DRIVEN METAL-INSULATOR TRANSITION

Figure 2(a) shows the partial occupation of oxygen and copper as a function of hole doping $\delta = 5 - n_{\rm tot}$ for $U_d = 12$ and

$\beta = 25$ (open symbols). In the undoped system, comparison with $U_d = 0$ (full symbols) shows that at finite U_d electrons are transferred from copper to oxygen. Lowering the chemical potential μ results in an essentially doping-independent n_d, while n_p decreases, indicating that the holes mainly enter the oxygen, as expected in the charge-transfer regime and found experimentally [11].

Figure 2(b) shows the doping as a function of μ for $U_d = 12$ and different temperatures. The plateau in the curves at $\delta(\mu) = 0$ reveals the onset of the incompressible charge-transfer insulator. By lowering μ until we obtain a compressible state, the isotherms $\delta(\mu)$ evolve continuously, i.e., without hysteresis. Hence we conclude that the transition between charge-transfer insulator and compressible phase is of second order at $T = 0$. The latter has the characteristics of a pseudogap phase, as discussed below. Upon doping further, a first-order transition occurs between that pseudogap phase and a more conventional correlated metal. Indeed, as T decreases, the isotherms $\delta(\mu)$ develop a sigmoidal shape and eventually hysteresis between two compressible solutions. This transition ends in a second-order critical point at (δ_p, T_p), at which thermodynamic response functions, such as the charge compressibility $\kappa = 1/n_{\rm tot}^2 (dn_{\rm tot}/d\mu)_T$, shown in Fig. 2(c) versus δ, diverge. For $T > T_p$, the two phases merge in a single supercritical phase, and the divergence in κ is replaced by a maximum value, which decreases with increasing T. It is striking that either below or above T_p, $(d\delta_{\rm tot}/dT)_\mu$ changes sign, from positive at small doping to negative at large doping, as can be seen from Fig. 2(b).

The emergent first-order transition at finite doping is connected to the charge-transfer insulator-to-metal transition in the undoped case. This can be deduced by tracking the position δ_p of the critical end point as a function of U_d, as shown by blue circles in Fig. 2(d). This line of critical end points (where the pseudogap-correlated metal transition ends) starts out at the metal-to-charge-transfer insulator transition at $\delta = 0$ and $U_d \simeq 11.6$ and moves progressively to high doping and lower T as U_d increases.

IV. PHASE DIAGRAM

The temperature-doping phase diagram shown in Fig. 3(a) summarizes the normal-state properties investigated so far. At zero doping, a second-order transition separates a charge-transfer insulating phase from a pseudogap phase. At finite doping, there is a first-order transition between two normal-state phases: the pseudogap and the correlated metallic state. [Lines with triangles are an estimate for the spinodal boundaries determined from the jumps in $\delta(\mu)$.] As the temperature increases, the first-order transition ends in a second-order critical point at (T_p, δ_p), where the thermodynamic response functions, such as the charge compressibility κ discussed above, diverge. For $T > T_p$, only one supercritical phase exists, but the first-order transition generates a crossover, the Widom line T_W, at which thermodynamic response functions show maxima. [The red line with circles is the line of maximum of κ computed in Fig. 2(c).] Quite generally, T_W marks also the border between different dynamic behaviors [29,30]: the drop in the local DOS goes through an inflection point

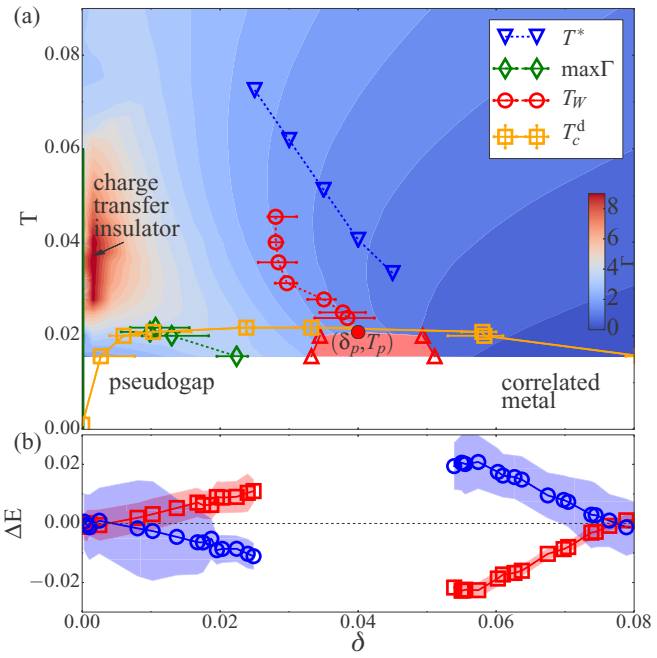

FIG. 3. (a) Temperature versus hole-doping phase diagram. Model parameters are $|\epsilon_p - \epsilon_d| = 9$, $t_{pp} = 1$, $t_{pd} = 1.5$, and $U_d = 12$. Four phases are shown. The d-wave superconducting phase is determined by a nonzero superconducting order parameter and is delimited by T_c^d (orange squares). The three normal-state phases are determined by the behavior of $\delta(\mu)$: CTI at $\delta = 0$, PG, and CM. Below T_c^d the normal state is metastable. PG and CM are separated by a first-order transition at finite doping (red triangles denote the jump in the occupation curves), terminating at a critical end point (δ_p, T_p) (full circle). Emanating from it is T_W, the crossover line of the maxima of the charge compressibility κ (open red circles), which is a proxy for the Widom line. Its high-temperature precursor is T^*, the line where the DOS at the Fermi level drops as a function of T (blue triangles). Color corresponds to the magnitude of the normal-state scattering rate Γ at cluster momentum $K = (\pi, 0)$. Green diamonds indicate the maximum of $\Gamma(\delta)|_T$ at low T and $\delta > 0$. (b) Difference in kinetic and potential energies between the superconducting and normal states (blue and red lines, respectively) versus δ at $\beta = 64$. Shaded regions give standard errors.

at T_W (SM Fig. 7 [27]). The onset of the drop in such quantity commonly defines the onset of the pseudogap T^* and occurs at the higher precursory temperature (see line with blue triangles and SM Fig. 7(c) [27]). This is qualitatively consistent with experiments [31]. The development of the pseudogap is characterized by the growth of intersite self-energies or, equivalently, by a strong momentum space differentiation of the electronic lifetimes (see SM Figs. 5 and 6 [27]). The first-order transition at finite doping between pseudogap and correlated metal, and its associated crossover, is the unifying feature of self-energy anisotropy, as can be seen by the ridge of large scattering rate $\Gamma_{K=(\pi,0)}$, shown as color plot in Fig. 3(a), emerging from $\delta_{c1}(T \to 0)$ and bent toward the charge-transfer insulator (line with green diamonds).

Proximity to Mott physics often entwines with broken symmetry states. While speculating that along the

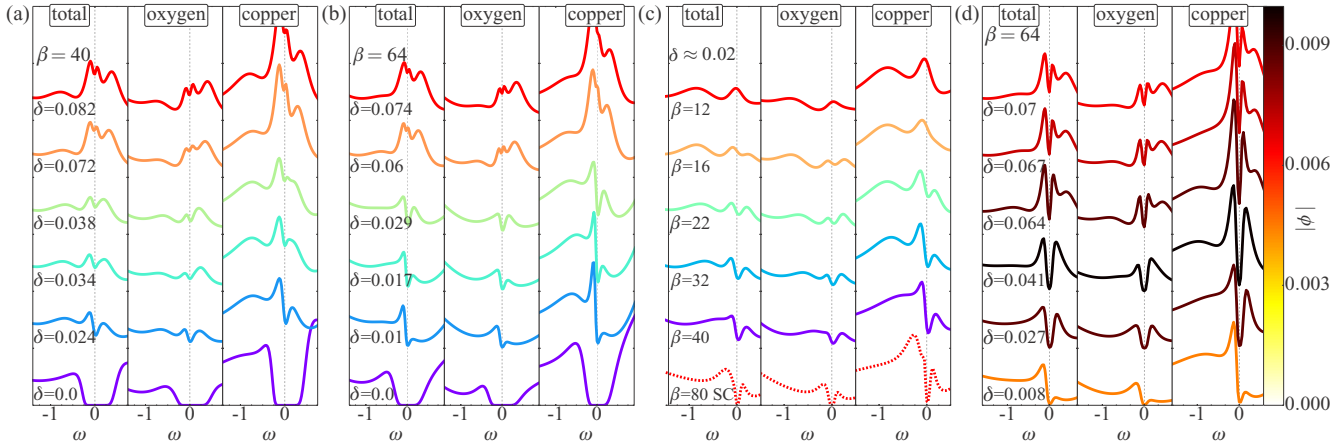

FIG. 4. Low-frequency part of the local DOS $N(\omega)$. Each DOS is normalized to unity. $N(\omega)_{\rm tot} = \frac{2}{3}N(\omega)_p + \frac{1}{3}N(\omega)_d$. (a,b) $N(\omega)$ for different dopings at constant inverse temperature (a) $\beta = 40 < 1/T_p$ and (b) $\beta = 64 > 1/T_p$. (c) $N(\omega)$ for different temperatures at constant doping $\delta \approx 0.02$. (d) $N(\omega)$ in the superconducting state at $\beta = 64$ for different dopings. In this panel, color corresponds to the magnitude of the superconducting order parameter.

charge-compressibility maxima T_W, the charge should be most susceptible to develop charge density modulations, we restrict our study to d-wave superconductivity. The dynamical mean-field superconducting transition temperature T_c^d [orange line in Fig. 3(a)] marks the temperature below which the superconducting order parameter is nonzero (see SM Fig. 13 [27]) and corresponds to the temperature below which Cooper pairs develop within the cluster. Complex behavior in the superconducting state originates from the underlying normal-state first-order transition: (a) T_c^d forms an asymmetric dome as a function of doping, whose broad maximum occurs close to the intercept of maximum Γ (green line). (b) T_W intercepts T_c^d, indicating that superconductivity and pseudogap are distinct phenomena, although they are entwined ones, since in our approach the origin of both phenomena is rooted in Mott physics. (c) For $\delta < \delta_p$, pairing is driven by kinetic energy, while for $\delta > \delta_p$ it is driven by potential energy, as illustrated in Fig. 3(b) by the difference of potential and kinetic energy between superconducting and normal states as a function of doping. This is qualitatively consistent with optical measurements [32,33].

The local DOS, shown in Fig. 4 (for the entire frequency spectrum, see SM Figs. 9–12 [27]), helps define the various phases. Figures 4(a) and 4(b) show the doping evolution of the normal-state DOS above and below T_p, respectively. Note the following: (i) At $\delta = 0$, $N(\omega)$ shows a correlation gap of charge-transfer type. (ii) Upon hole doping, a dramatic redistribution of spectral weight occurs in $N(\omega)$ as a consequence of electronic correlations. At low frequency $N(\omega)$ develops a pseudogap having a large Cu character with significant O component [22,34]. The frequency profile has a large particle-hole asymmetry, qualitatively similar to experimental observation [35]. (iii) Increasing δ further, particle-hole asymmetry is reduced, the spectral weight inside the pseudogap progressively fills in, eventually the pseudogap disappears, and a broad peak at the Fermi level takes shape.

Figure 4(c) shows the temperature evolution of $N(\omega)$ for $\delta < \delta_p$ and demonstrates that the pseudogap gradually fills in upon raising T, in qualitative agreement with experiment [36]. Last, Fig. 4(d) shows $N(\omega)$ in the superconducting state for several dopings. The coherence peaks are visible both in Cu and O partial DOS, demonstrating that Cooper pairs are composite objects of mixed d-p character. This feature is reminiscent of "Zhang-Rice singlet" physics [34].

The present study shows that an antiferromagnetic quantum critical point [37] is not necessary to obtain pseudogap or d-wave superconductivity. The interplay with other broken-symmetry phases, such as charge density waves [38–40] or loop currents [41–46], are important issues to be considered in subsequent investigations.

V. SUMMARY

In summary, we charted the phase diagram of a hole-doped charge-transfer insulator using a three-band model solved with CDMFT. We revealed the structure of both the normal and superconducting phases, and fingerprinted their organizing principle as a normal-state first-order transition below the superconducting dome. This transition is analog to the one found in the single-band Hubbard model [30,47–51], despite the large differences in microscopic details, namely, the presence of oxygen, the different band structure, and the energy redistribution of spectral weight. This suggests the emergent character of the phenomenon, solely produced by Mott physics plus short-range correlations, and thus leads to the following conjecture: a first-order transition, even when hidden by another phase, here superconductivity, can act as a general organizing principle of strongly coupled matter. In solids this is now clear for systems described by Hubbard-like models [30,51–56], in fluids it has been suggested before [29,57,58], and in quark matter the putative critical end point in the T vs baryon chemical potential that appears in the QCD phase diagram may be another manifestation of the generality of this phenomenon in strongly interacting systems [59–61].

ACKNOWLEDGMENTS

We acknowledge D. Sénéchal, G. Kotliar, M. Rozenberg, and Y. Sidis for discussions. This work was partially supported by the Natural Sciences and Engineering Research Council (Canada), the Tier I Canada Research Chair Program (A.-M.S.T.), and Université de Sherbrooke. Simulations were performed on computers provided by Canadian Foundation for Innovation, Ministère de l'Éducation des Loisirs et du Sport (Québec), Calcul Québec, and Compute Canada.

[1] B. Keimer, S. A. Kivelson, M. R. Norman, S. Uchida, and J. Zaanen, Nature (London) **518**, 179 (2015).
[2] P. W. Anderson, Science **235**, 1196 (1987).
[3] T. Maier, M. Jarrell, T. Pruschke, and M. H. Hettler, Rev. Mod. Phys. **77**, 1027 (2005).
[4] G. Kotliar, S. Y. Savrasov, K. Haule, V. S. Oudovenko, O. Parcollet, and C. A. Marianetti, Rev. Mod. Phys. **78**, 865 (2006).
[5] A.-M. S. Tremblay, B. Kyung, and D. Sénéchal, Low Temp. Phys. **32**, 424 (2006).
[6] A. Georges, G. Kotliar, W. Krauth, and M. J. Rozenberg, Rev. Mod. Phys. **68**, 13 (1996).
[7] E. Gull and A. J. Millis, Nat. Phys. **11**, 808 (2015).
[8] A.-M. S. Tremblay, in *Emergent Phenomena in Correlated Matter Modeling and Simulation*, edited by E. Pavarini, E. Koch, and U. Schollwöck (Verlag des Forschungszentrum, Jülich, 2013), Vol. 3, Chap. 10.
[9] V. J. Emery, Phys. Rev. Lett. **58**, 2794 (1987).
[10] C. Varma, S. Schmitt-Rink, and E. Abrahams, Solid State Commun. **62**, 681 (1987).
[11] N. Gauquelin, D. G. Hawthorn, G. A. Sawatzky, R. X. Liang, D. A. Bonn, W. N. Hardy, and G. A. Botton, Nat. Commun. **5**, 4275 (2014).
[12] J. Zaanen, G. A. Sawatzky, and J. W. Allen, Phys. Rev. Lett. **55**, 418 (1985).
[13] A. Georges, G. Kotliar, and W. Krauth, Z. Phys. B: Condens. Matter **92**, 313 (1993).
[14] P. Lombardo, M. Avignon, J. Schmalian, and K.-H. Bennemann, Phys. Rev. B **54**, 5317 (1996).
[15] M. Zölfl, T. Maier, T. Pruschke, and J. Keller, Eur. Phys. J. B **13**, 47 (2000).
[16] G. Sordi, A. Amaricci, and M. J. Rozenberg, Phys. Rev. Lett. **99**, 196403 (2007).
[17] C. Weber, K. Haule, and G. Kotliar, Phys. Rev. B **78**, 134519 (2008).
[18] C. Weber, K. Haule, and G. Kotliar, Nat. Phys. **6**, 574 (2010).
[19] L. de' Medici, X. Wang, M. Capone, and A. J. Millis, Phys. Rev. B **80**, 054501 (2009).
[20] X. Wang, L. de' Medici, and A. J. Millis, Phys. Rev. B **83**, 094501 (2011).
[21] X. Wang, H. T. Dang, and A. J. Millis, Phys. Rev. B **84**, 014530 (2011).
[22] A. Macridin, M. Jarrell, T. Maier, and G. A. Sawatzky, Phys. Rev. B **71**, 134527 (2005).
[23] E. Arrigoni, M. Aichhorn, M. Daghofer, and W. Hanke, New J. Phys. **11**, 055066 (2009).
[24] C. Weber, C. Yee, K. Haule, and G. Kotliar, Europhys. Lett. **100**, 37001 (2012).
[25] A. Go and A. J. Millis, Phys. Rev. Lett. **114**, 016402 (2015).
[26] O. Andersen, A. Liechtenstein, O. Jepsen, and F. Paulsen, J. Phys. Chem. Solids **56**, 1573 (1995).
[27] See Supplemental Material at http://link.aps.org/supplemental/10.1103/PhysRevB.93.245147 for details of model and method, including Fermi surface and band structure; complementary data on the doping-driven metal to insulator transition, in particular the temperature and doping dependence of the compressibility, scattering rates and average sign; and the full frequency spectrum of the local DOS along with the superconducting order parameter as a function of doping for a few temperatures.
[28] E. Gull, A. J. Millis, A. I. Lichtenstein, A. N. Rubtsov, M. Troyer, and P. Werner, Rev. Mod. Phys. **83**, 349 (2011).
[29] L. Xu, P. Kumar, S. V. Buldyrev, S.-H. Chen, P. H. Poole, F. Sciortino, and H. E. Stanley, Proc. Natl. Acad. Sci. USA **102**, 16558 (2005).
[30] G. Sordi, P. Sémon, K. Haule, and A.-M. S. Tremblay, Sci. Rep. **2**, 547 (2012).
[31] H. Alloul, C. R. Phys. **15**, 519 (2014).
[32] H. J. A. Molegraaf, C. Presura, D. van der Marel, P. H. Kes, and M. Li, Science **295**, 2239 (2002).
[33] C. Giannetti, F. Cilento, S. D. Conte, G. Coslovich, G. Ferrini, H. Molegraaf, M. Raichle, R. Liang, H. Eisaki, M. Greven, A. Damascelli, D. van der Marel, and F. Parmigiani, Nat. Commun. **2**, 353 (2011).
[34] F. C. Zhang and T. M. Rice, Phys. Rev. B **37**, 3759 (1988).
[35] Y. Kohsaka, C. Taylor, K. Fujita, A. Schmidt, C. Lupien, T. Hanaguri, M. Azuma, M. Takano, H. Eisaki, H. Takagi, S. Uchida, and J. C. Davis, Science **315**, 1380 (2007).
[36] T. Timusk and B. Statt, Rep. Prog. Phys. **62**, 61 (1999).
[37] A. V. Chubukov, D. Pines, and J. Schmalian, *Superconductivity: Conventional and unconventional superconductors* (Springer, Berlin, 2008), pp. 1349–1413.
[38] K. B. Efetov, H. Meier, and C. Pepin, Nat. Phys. **9**, 442 (2013).
[39] S. Sachdev and R. La Placa, Phys. Rev. Lett. **111**, 027202 (2013).
[40] Y. Wang and A. Chubukov, Phys. Rev. B **90**, 035149 (2014).
[41] C. M. Varma, P. B. Littlewood, S. Schmitt-Rink, E. Abrahams, and A. E. Ruckenstein, Phys. Rev. Lett. **63**, 1996 (1989).
[42] C. M. Varma, Phys. Rev. B **73**, 155113 (2006).
[43] C. Weber, T. Giamarchi, and C. M. Varma, Phys. Rev. Lett. **112**, 117001 (2014).
[44] S. Bulut, A. P. Kampf, and W. A. Atkinson, Phys. Rev. B **92**, 195140 (2015).
[45] Y. F. Kung, C.-C. Chen, B. Moritz, S. Johnston, R. Thomale, and T. P. Devereaux, Phys. Rev. B **90**, 224507 (2014).
[46] V. S. de Carvalho, C. Pépin, and H. Freire, Phys. Rev. B **93**, 115144 (2016).
[47] G. Sordi, K. Haule, and A.-M. S. Tremblay, Phys. Rev. Lett. **104**, 226402 (2010).
[48] G. Sordi, K. Haule, and A.-M. S. Tremblay, Phys. Rev. B **84**, 075161 (2011).

[49] G. Sordi, P. Sémon, K. Haule, and A.-M. S. Tremblay, Phys. Rev. Lett. **108**, 216401 (2012).
[50] G. Sordi, P. Sémon, K. Haule, and A.-M. S. Tremblay, Phys. Rev. B **87**, 041101 (2013).
[51] L. Fratino, P. Sémon, G. Sordi, and A.-M. S. Tremblay, Sci. Rep. **6**, 22715 (2016).
[52] T. Furukawa, K. Miyagawa, H. Taniguchi, R. Kato, and K. Kanoda, Nat. Phys. **11**, 221 (2015).
[53] H. Terletska, J. Vučičević, D. Tanasković, and V. Dobrosavljević, Phys. Rev. Lett. **107**, 026401 (2011).
[54] J. Vučičević, H. Terletska, D. Tanasković, and V. Dobrosavljević, Phys. Rev. B **88**, 075143 (2013).
[55] J. Vučičević, D. Tanasković, M. J. Rozenberg, and V. Dobrosavljević, Phys. Rev. Lett. **114**, 246402 (2015).
[56] C.-D. Hébert, P. Sémon, and A.-M. S. Tremblay, Phys. Rev. B **92**, 195112 (2015).
[57] P. F. McMillan and H. E. Stanley, Nat. Phys. **6**, 479 (2010).
[58] G. G. Simeoni, T. Bryk, F. A. Gorelli, M. Krisch, G. Ruocco, M. Santoro, and T. Scopigno, Nat. Phys. **6**, 503 (2010).
[59] R. A. Lacey, Phys. Rev. Lett. **114**, 142301 (2015).
[60] M. Stephanov, K. Rajagopal, and E. Shuryak, Phys. Rev. Lett. **81**, 4816 (1998).
[61] M. Stephanov, Prog. Theor. Phys. Suppl. **153**, 139 (2004).